Supplementary Information

1 Calibration of empirical scaling relationships

The empiric laws used to correlate the P-wave parameters to the PGV, and the magnitude were calibrated using seismic events that happened in the region after the main event (Supplementary Table 1). We started from accelerometric traces and then obtained the values in velocity and displacement after one and then two numerical integrations. Every trace was manually picked and then to calculate the P-wave parameters, a variable time window from the P pick to the theoretical S-wave arrival, was used.

Supplementary Table S1. This table shows the date and the source location and magnitude parameters of the events used to calibrate the P-wave ground motion empirical equations (eq. S1, eq. S2).

Event Origin Time	latitude (deg)	longitude (deg)	Depth (km)	Moment Magnitude
03/05/2023 06:20:52 (UTC)	37.606	35.530	13.13	4.3
27/02/2023 02:51:20 (UTC)	37.932	37.584	8.51	5.0
23/02/2023 15:53:47 (UTC)	38.272	38.303	6.15	5.6
06/02/2023 01:28:16 (UTC)	36.893	37.189	9.8	6.6
06/02/2023 10:24:48 (UTC)	37.239	38.089	7.0	7.6
06/02/2023 01:17:34 (UTC)	37.226	37.014	10.0	7.8

The accelerograms of these events recorded by the AFAD network were used to determine the coefficients of the relationship between the moment magnitude (M_w) and the on the P waves peak amplitudes (P_x) and the hypocentral distance (R_H).

$$M_w = A_x + B_x * \log_{10} P_x + C_x * \log_{10} R_H \qquad (S1)$$

where x=a,v,d; a=acceleration, v=velocity, d=displacement. The coefficients A_x, B_x and C_x are given in Supplementary Table S2.

Supplementary Table S2. Coefficients of the empirical relationships S1.

Acceleration (P_a)	$\boldsymbol{A_a}$	$\boldsymbol{C_a}$	$\boldsymbol{C_a}$
	2.6 ± 0.2	1.07 ± 0.03	1.5 ± 0.1
Velocity (P_v)	$\boldsymbol{A_v}$	$\boldsymbol{C_v}$	$\boldsymbol{C_v}$
	3.9 ± 0.2	1.11 ± 0.04	1.3 ± 0.1
Displacement (P_d)	$\boldsymbol{A_d}$	$\boldsymbol{C_d}$	$\boldsymbol{C_d}$
	4.8 ± 0.3	0.88 ± 0.04	1.2 ± 0.1

In Supplementary Figure S1 we show eq. S1 compared with the data we used for the calibration.

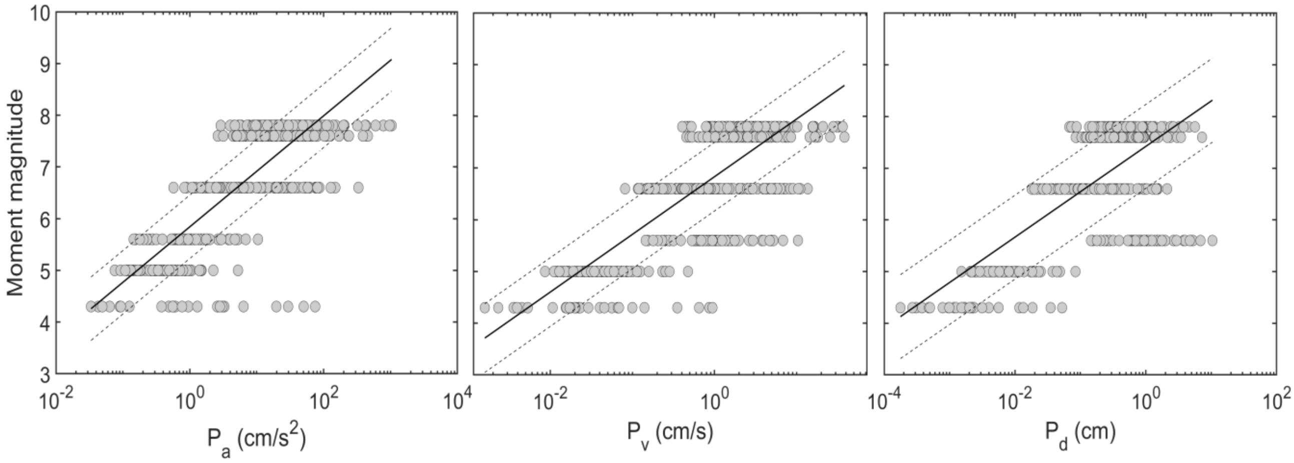

Supplementary Figure S1. Data from events in table 1S (grey dots). In this figure we fixed the hypocentral distance at 150 km to show the interpolated law (black solid line) with its uncertainty (black dashed lines).

The same events in Supplementary Table 1 were used to calibrate the following empiric relationship:

$$\log_{10} PGV = A'_x + B'_x * \log_{10} P_x \qquad (S2)$$

where x=a,v,d; a=acceleration, v=velocity, d=displacement. The coefficients A_x, B_x and C_x are given in Supplementary Table S3.

Supplementary Table S3. Table showing coefficients for equation 2S for all the three parameters mentioned before.

Acceleration (P_a)	A'_a	B'_a
	-0.76 ± 0.01	0.99 ± 0.01
Velocity (P_v)	A'_v	B'_v
	0.16 ± 0.02	1.01 ± 0.02
Displacement (P_d)	A'_d	B'_d
	0.69 ± 0.04	0.77 ± 0.04

In Supplementary Figure S2 we show log PGV vs log Px law S1 compared with the data used for the coefficient determination of the empirical relation (S2).

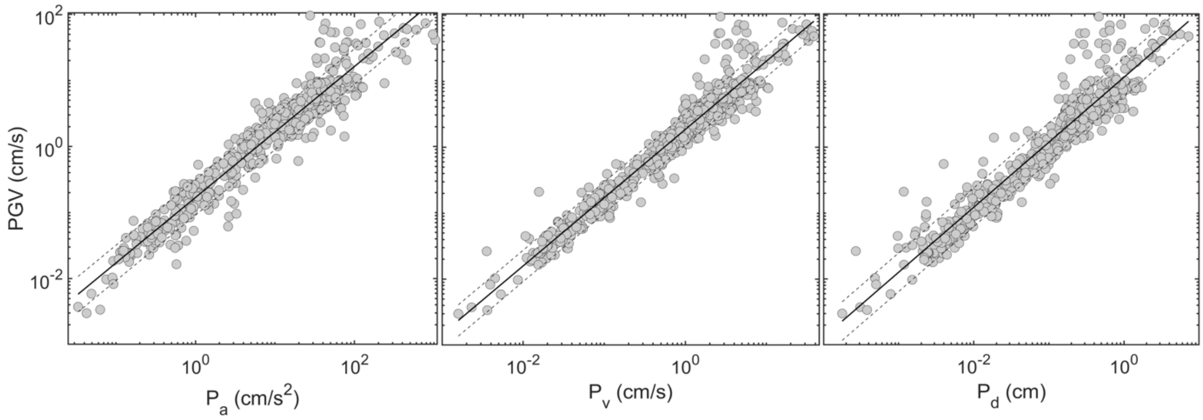

Supplementary Figure S2. Empirical scaling relationships. The figure shows the $log(PGV)\, vs\, log\,(P_x)$ (x=a (acceleration), v (velocity), d (displacement)) empirical scaling relationships. Grey dots indicate the data from 6 events in the region. The solid black line is the linear regression relationships, and the dashed lines represent the standard error on this law.

2 Performance analysis with different PGV-to-I_{MM} scaling relationships

In the main text we show the performance results using the Intensity scale of Faenza and Michelini[1], but different intensity scales can be used. This changes the thresholds in PGV corresponding to the thresholds in intensity. The choice of intensity scale must be adapted to the buildings the user wants to protect, because, in different areas of the world, the quality and the strength of the buildings can change. In the following figures we show results obtained using thresholds IV and VI on the scale by Warden et al.[2] (**Supplementary Figures S3, S4, S5**) and Bilal & Askan[3] (**Supplementary Figures S6, S7, S8**). The first one is used by USGS for events all over the world, while the second one is specific for Turkish region. Using the scale by Warden et al.[2] we retrieved a large number of successful alerts (over 80% at 25s from origin time) for the lower threshold, while for the higher threshold at the beginning we have more than 50% of the station successfully non alerted (**Supplementary Figure S3**). The lead times available are very different using the two thresholds (**Supplementary Figure S4**). In fact, the predicted PGV exceeds the threshold for almost all the stations for the I_{MM}=IV (resulting in lead time greater than 110 s for epicentral distance of 280 km), while the system needs more time to predict the exceeding of IMM=VI. In general, we need that the P-wave reaches the site to have this prediction (resulting in shorter lead times, for example about 20 s at 150 km of epicentral distance). This is evident in **Supplementary Figure S5.** Using the scale by Bilal & Askan[3], we have a majority of missed alerts (almost 80% for IMM=IV and more than 50% for IMM=VI) at the time of first alert (**Supplementary Figure S6**). This is because the system needs time to reach an estimated magnitude value greater than 7 (see main text), due to the nature of the event. Clearly this has an effect also on the lead times. In **Supplementary Figure S7,** in fact, we see how the predicted intensity exceeds the threshold farther and farther from the epicenter as the time goes on. Nevertheless, we have good results for lead times using both thresholds (up to 50 s at 150 km for IMM=IV and up to 30 s at 150 km for IMM=VI). Using the higher intensity threshold the system needs the P-wave to reach the site to correctly predict the PGV as for the previous case (**Supplementary Figure S8**).

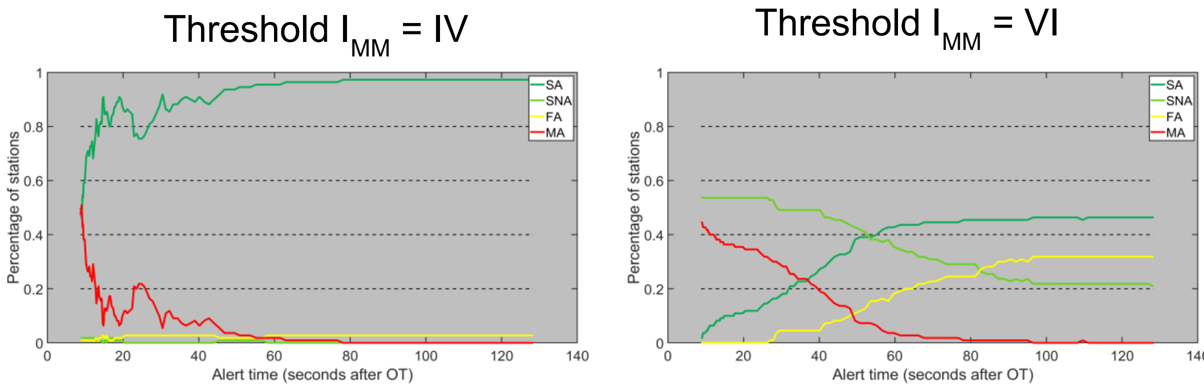

Supplementary Figure S3. Figure showing the percentage of stations classified as MA, FA, SA, SNA for the two chosen intensity thresholds.

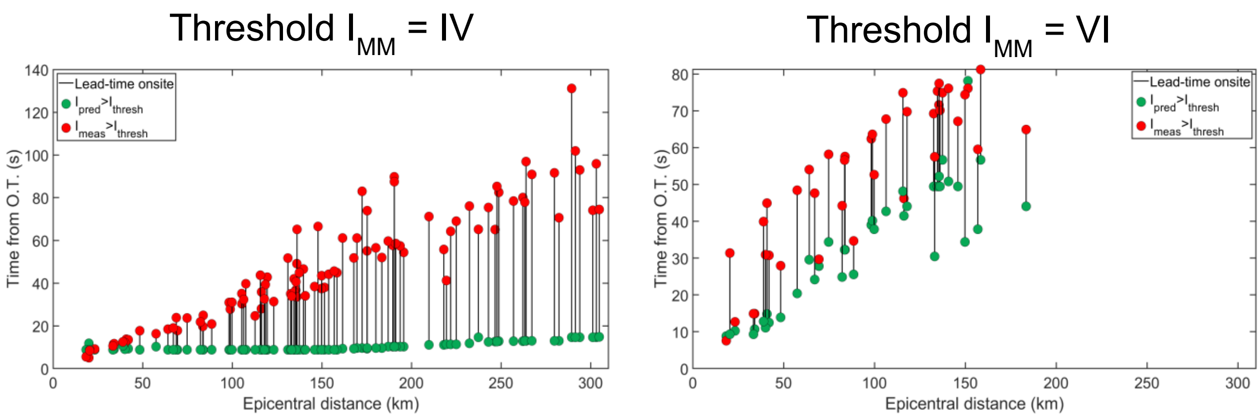

Supplementary Figure S4. The figure shows the lead time at each station versus the epicentral distance. The time at which the predicted PGV exceeds the threshold is indicated with green circles while the time at which the measured PGV exceeds the same threshold is indicated with red circles. The segments connecting the points represents the lead-time that the station have, to take mitigation actions.

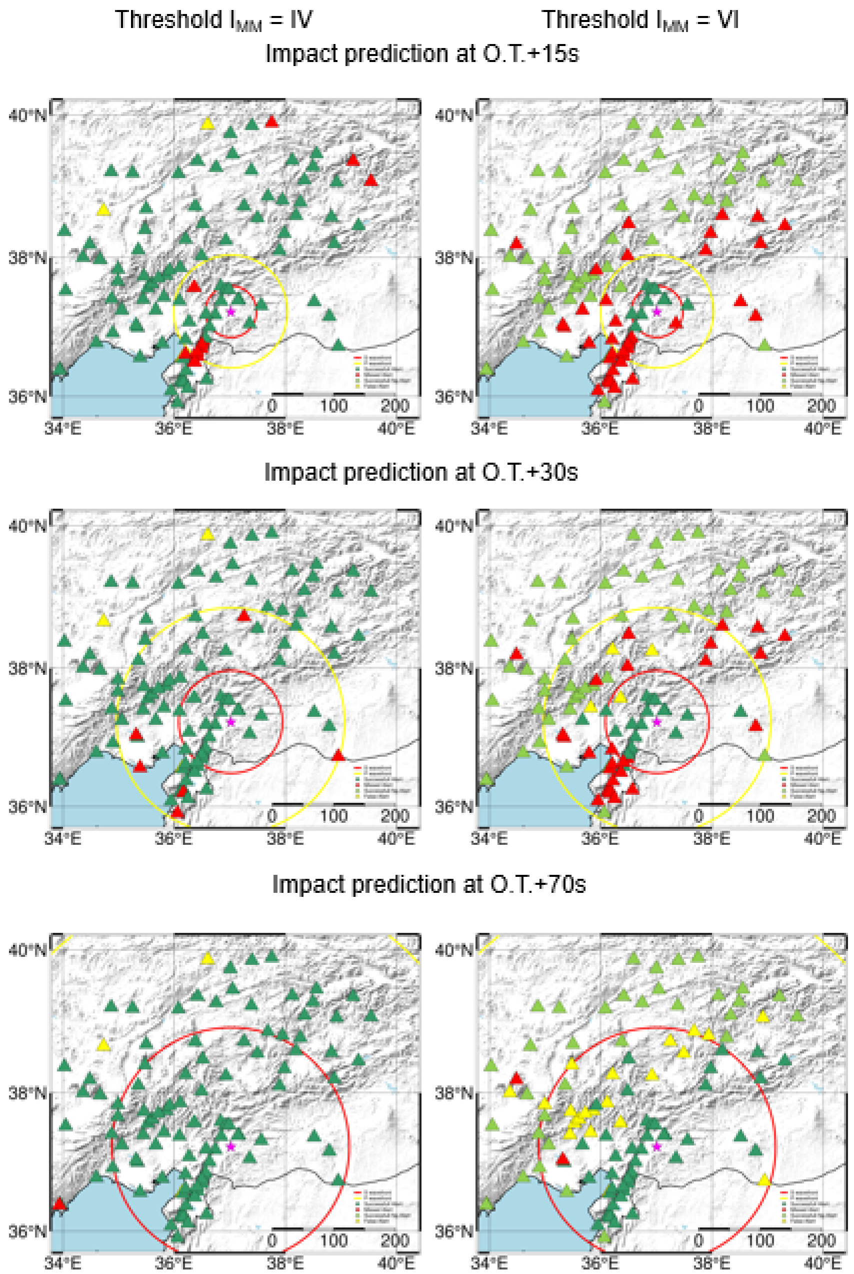

Supplementary Figure S5. Maps of the impact prediction in terms of successful, misses and false alerts at three different times after OT and for the two considered I_{MM}=IV and I_{MM}=VI thresholds for the alert. Every station in the area is represented as a triangle with a different color based on the alert, while the epicenter is indicated with a magenta star. The red circle represents the S-wavefront, and the yellow circle represents the P-wavefront.

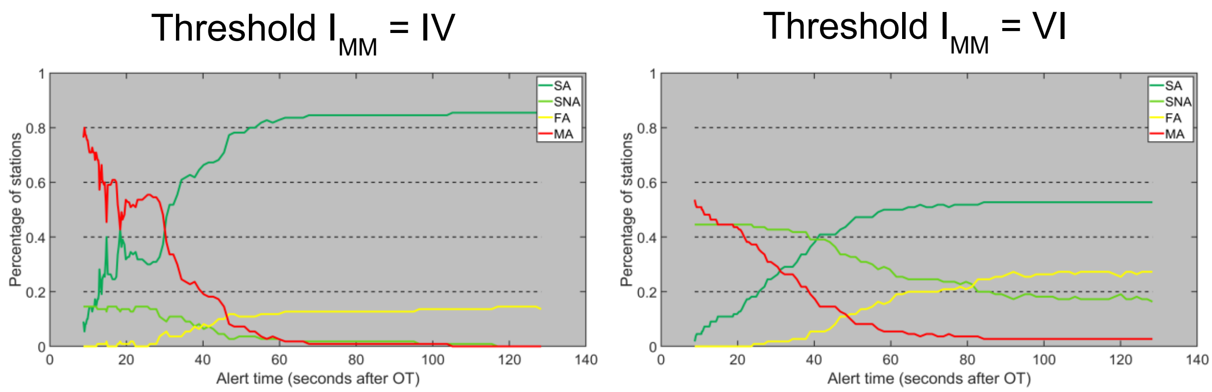

Supplementary Figure S6. Percentage of stations classified as SA, MA, SNA, FA in time for the two intensity thresholds.

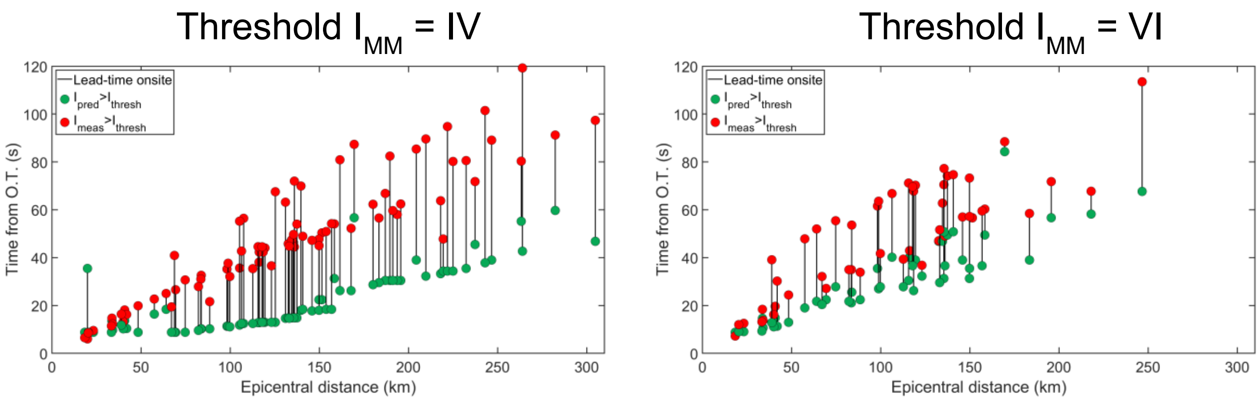

Supplementary Figure S7. The figure shows the lead time at each station versus the epicentral distance. The time at which the predicted PGV exceeds the threshold is indicated with green circles while the time at which the measured PGV exceeds the same threshold is indicated with red circles. The segments connecting the points represents the lead-time that the station have, to take mitigation actions.

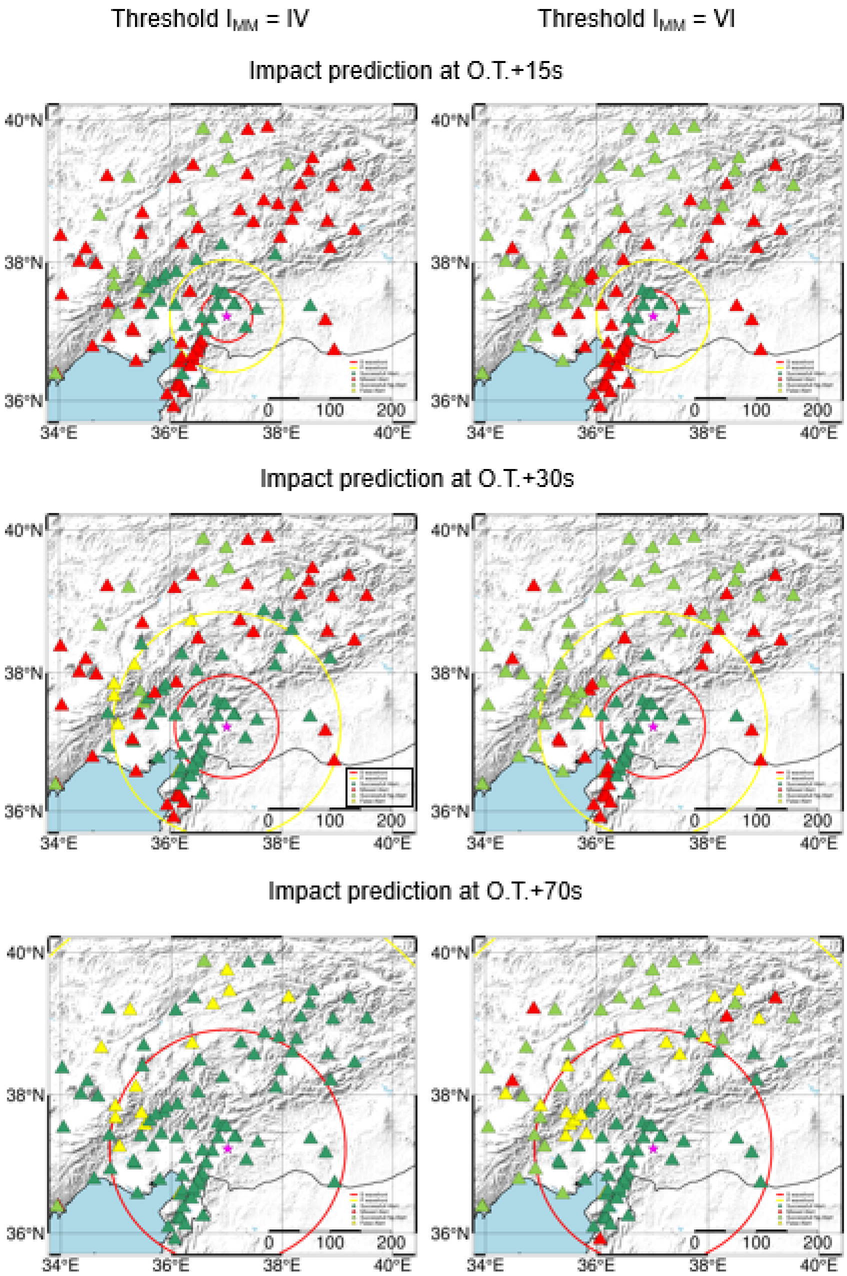

Supplementary Figure S8. Maps of the impact prediction in terms of successful, misses and false alerts at three different times after OT and for the two considered I_{MM}=IV and I_{MM}=VI thresholds for the alert. Every station in the area is represented as a triangle with a different color based on the alert, while the epicenter is indicated with a magenta star. The red circle represents the S-wavefront, and the yellow circle represents the P-wavefront.

Bibliography of the Supplementary Information Material

1. Licia Faenza, Alberto Michelini, Regression analysis of MCS intensity and ground motion parameters in Italy and its application in ShakeMap, *Geophysical Journal International*, Volume 180, Issue 3, March 2010, Pages 1138–1152, https://doi.org/10.1111/j.1365-246X.2009.04467.x
2. C. B. Worden, M. C. Gerstenberger, D. A. Rhoades, D. J. Wald; Probabilistic Relationships between Ground-Motion Parameters and Modified Mercalli Intensity in California. *Bulletin of the Seismological Society of America* 2012; 102 (1): 204–221. https://doi.org/10.1785/0120110156
3. Bilal, M., Askan, A. Relationships between Felt Intensity and Recorded Ground-Motion Parameters for Turkey (2014). *Bulletin of the Seismological Society of America*; 104 (1): 484–496. https://doi.org/10.1785/0120130093